Biochimica et Biophysica Acta 1787 (2009) 183–190

Contents lists available at ScienceDirect

Biochimica et Biophysica Acta

journal homepage: www.elsevier.com/locate/bbabio

De-novo modeling and ESR validation of a cyanobacterial F_oF_1–ATP synthase subunit *bb′* left-handed coiled coil ☆

Oleg A. Volkov [a], Tarek M. Zaida [a], Petra Voeller [b], Holger Lill [b], John G. Wise [a], Pia D. Vogel [a,*]

[a] Department of Biological Sciences, Southern Methodist University, Dallas, TX 75275, USA
[b] Institute of Molecular Cell Biology, Department of Structural Biology, Vrije Universiteit, De Boelelaan 1087, 1081 HV Amsterdam, The Netherlands

ARTICLE INFO

Article history:
Received 12 November 2008
Received in revised form 12 December 2008
Accepted 15 December 2008
Available online 25 December 2008

Keywords:
ATPase
External stalk
b-subunit
Coiled coil
De-novo modeling
Site-specific spin labeling
ESR spectroscopy

ABSTRACT

The structure and functional role of the dimeric external stalk of F_oF_1–ATP synthases have been very actively researched over the last years. To understand the function, detailed knowledge of the structure and protein packing interactions in the dimer is required. In this paper we describe the application of structural prediction and molecular modeling approaches to elucidate the structural packing interaction of the cyanobacterial ATP synthase external stalk. In addition we present biophysical evidence derived from ESR spectroscopy and site directed spin labeling of stalk proteins that supports the proposed structural model. The use of the heterodimeric *bb′* dimer from a cyanobacterial ATP synthase (*Synechocystis* sp. PCC 6803) allowed, by specific introduction of spin labels along each individual subunit, the evaluation of the overall tertiary structure of the subunits by calculating inter-spin distances. At defined positions in both *b* and *b′* subunits, reporter groups were inserted to determine and confirm inter-subunit packing. The experiments showed that an approximately 100 residue long section of the cytoplasmic part of the *bb′*-dimer exists mostly as an elongated α-helix. The distant C-terminal end of the dimer, which is thought to interact with the δ-subunit, seemed to be disordered in experiments using soluble *bb′* proteins. A left-handed coiled coil packing of the dimer suggested from structure prediction studies and shown to be feasible in molecular modeling experiments was used together with the measured inter-spin distances of the inserted reporter groups determined in ESR experiments to support the hypothesis that a significant portion of the *bb′* structure exists as a left-handed coiled coil.

1. Introduction

F_oF_1–ATP synthases provide the bulk of ATP that is needed for metabolic and catabolic processes as well as for cellular and organismal movement [1–3]. The synthase is found in the energy coupling membranes of thylakoid membranes, the mitochondrial inner membranes and the plasma membranes of bacteria. The subunit stoichiometry of the membrane-embedded F_o sector was reported to be 10–15 copies of subunit *c* for synthases of different origin, one subunit *a*, and one or two subunits *b* that make up much of the external stalk linking F_o to the catalytically active F_1-ATPase. F_1 contains five conserved subunits arranged in an $\alpha_3\beta_3\gamma\delta\varepsilon$ complex. Eubacterial ATP synthases contain two identical subunits *b* while photosynthetic organisms contain heterodimeric *bb′* subunits (called subunits I and II in chloroplast ATP synthase). Mitochondrial ATP synthases contain only one subunit *b*, but other subunits (*d* and F_6) are present that stabilize the overall external stalk–stator structure (for recent reviews see [4–6]). Subunit δ (OSCP in mitochondrial enzymes) seems to facilitate and strengthen the link between the *b*-dimer and the F_1-part of the enzyme [7].

The F_o-sector enables proton translocation across the energy coupling membrane down an electrochemical gradient and couples, via rotation of the ring of subunits *c*, the energy of the proton gradient to the energy needed for ATP product release from F_1 during catalysis. The rotary motions within F_o and F_1 mesh with different step sizes. Rotation of the subunit *c* ring occurs with steps between 36° and 24° per translocated proton. The rotational steps of subunit γ were shown to be distinct 120° steps for one ATP synthesis or ATP hydrolysis event [8–10]. The mechanism of the gearing of these different rotational movements is not only of great significance to the overall mechanism of the ATP synthase, it is also of great interest from engineering points of view due to the extremely high thermodynamic efficiency of this rotary motor [11].

A major player that may link these rotations is the stator subunit *b* dimer, which connects the non-rotating F_o subunit *a* to the non-rotating F_1 subunits ($\alpha_3\beta_3$). The *bb* or *bb′* dimer may also closely contact the rotating *c*-subunit ring as well as the rotating ε-subunit of

☆ This work was supported by grant from the National Science Foundation (MCB 0415713) to PDV.

* Corresponding author. Department of Biological Sciences, Southern Methodist University, 6501 Airline Road, Dallas, TX 75275, USA. Tel.: +1 214 768 1790; fax: +1 214 768 3955.
E-mail address: pvogel@smu.edu (P.D. Vogel).

0005-2728/$ – see front matter © 2008 Elsevier B.V. All rights reserved.
doi:10.1016/j.bbabio.2008.12.007

F_1. It seems plausible that elastic conformational changes of the *b*-dimer may be involved in coupling the unequal rotational steps of F_o- and F_1-subunits [12]. Alternatively, the elasticity may take the form of winding or unwinding of the motor subunit γ coiled coil structure itself and not require additional participation by the external stalk. Combinations of both alternatives may also occur. Testing these models requires knowledge of conformational changes of the *b*-dimer during catalytic turnover. The prerequisite for these studies is a detailed knowledge of the structure and dimer packing of the external stalk.

X-ray structural models of the external stalk of the mitochondrial subunit complex bdF_6 were reported that show close packing of the stalk onto the surface of F_1 [13–15]. That the bdF_6 complex crystallized in such a perfectly F_1-complementary structure suggests that the external stalk may function as a rigid stator into which little energy from rotational steps could be transferred and later recovered. This may imply that the energies of intermediate steps required for coupling stem more from elastic deformations of subunit γ during catalysis. Experiments using bacterial ATPases, however, showed an unprecedented degree of structural plasticity in the *b*-homodimer. Almost 10% of the overall length of the protein could be deleted or inserted while still maintaining function [16,17]. Even *b*-subunits of unequal length retained catalytic activity [18]. Parts of the *b*-dimer could be exchanged for *b*-sequences from different species without complete loss of activity, although it is worthwhile to note that the parts of *b* thought to interact directly with F_1 were not interchangeable [19]. Tight interaction of the *b*-dimer with F_1 had previously been mapped to the C-terminal half of the *Escherichia coli* stator [20].

Controversy still exists about the packing of homodimeric *bb* structure, and much remains to be learned about the heterodimeric *bb′* external stalks from photosynthetic organisms. An X-ray structural model of a monomeric *E. coli b*-subunit dimerization domain was presented by the Dunn laboratory [21]. Visual inspection of a putative dimerization interface led the authors to speculate that *b* forms a right handed dimeric coiled coil. Right-handed coiled coil helical packing has been predicted to occur when interface residues occur in undecad (11-residue) repeats, allowing close packing interactions of *a* and *h* positions, usually occupied by small amino acid side chains, and *d* and *e* positions that are more peripheral and accommodate larger side chains [22]. So far no right-handed *dimeric* coiled coil has been shown to stably exist although trimers and tetramers have been observed. The dimeric right handed coiled coil therefore remains hypothetical. The X-ray model of the *b*-monomer [21] did, however, trigger a series of cysteine cross-linking studies from Dunn et al. that have been interpreted as supporting an unusual staggered right-handed homodimeric coiled coil [23,24].

The experimental protocols reported in these cross-linking studies show that very long incubation times under oxidative conditions were employed (either 24 h of rigorous stirring in the presence of air and $CuCl_2$ [23] or 72 h of dialysis in $CuCl_2$ solutions [24]). Excess cysteine in the experiments was intended to prevent non-specific cross-links. It seems very likely that during the extended incubation times employed the protective cysteine would have oxidized to cystine. Lack of reversibility of the cross-linking reactions and the long reaction times would in our estimation lead to accumulation of cross-linked products that reflected good disulfide formation chemistry but not necessarily stable low energy protein conformations. Oxidation of cysteines might in fact be obtained only in rarely occupied protein conformational states that present optimal reaction orientations of the cysteines. For these reasons we believe interpretation of these results should be viewed with caution. The results of these studies were interpreted by Dunn et al. [23,24] to indicate cross-links between introduced cysteines with an off-set of 4, 7 or 11 amino acids. These offsets would represent approximately one, two or three helical turns, respectively, between similar interfacial positions. It should be noted that only an offset of 11-residues is consistent with an uninterrupted right-handed coiled coil in this region as also proposed by Dunn.

A different approach to elucidating the *b* dimer structure was performed recently by our group [25,26]. We used structure prediction programs that identified extensive heptad repeat sequences in *b*-subunits from a variety of ATP synthases. Heptad repeats are often indicative of the propensity to form left-handed coiled coils. Molecular modeling strongly suggested that the *E. coli* subunit *b* dimer could fold into left-handed coiled coil structures [26]. These left-handed coiled coil models could be superposed with the monomeric subunit *b* X-ray structural model from Dunn [21], supporting further the validity of the left-handed coiled coil model. Experimental support for the left-handed coiled coil model was obtained by the excellent fit of 38 inter-subunit distance restraints that were obtained after site-specific spin-labeling of introduced cysteine residues and from ESR spectroscopy analyses [25].

In this report we describe enhanced efforts to obtain structural information about the external stalk of F_1F_o–ATP synthases. In these new studies we used a heterodimeric *bb′* from a cyanobacterial ATP synthase. This allowed us to acquire both intra- and intermolecular ESR-derived distance data since *b* and *b′* are encoded by different genes and allowed insertion of reporter groups either within one of the dimers or in each of the subunits independently. Structure prediction and improved modeling techniques emphasizing classic knobs in holes packing predicted by Crick [27] strongly suggested that the cyanobacterial *bb′* dimer can form, similar to the homologous *E. coli b*-homodimer, a stable, left handed coiled coil structure. Experimentally determined intra- and inter-chain distances agreed with distances obtained in molecular models of the spin-labeled proteins. These results strongly support the hypothesis that the external *bb′* stalk can adopt a left-handed, unstaggered coiled coil structure.

2. Materials and methods

2.1. Expression plasmids

The polar domains of subunit *b* (residues 49–179) and *b′* (residues 30–143) from the cyanobacterium *Synechocystis* sp. PCC 6803 ATP synthase were expressed using the plasmids pETb_{sol} and pETb'_{sol} [28]. Both subunits contained N-terminal His-6 or His-10 tags for easier purification. Single cysteine mutations were introduced using the Quikchange™ mutagenesis kit (Stratagene). The success of the mutation reactions was verified by DNA sequencing.

2.2. Protein expression

The wild-type and mutant polar domains of the subunits *b* and *b′* were expressed individually in *E. coli* strain BL21 (DE3) (Stratagene). The cells were grown in LB medium at 37 °C and constant shaking of 300 rpm. The expression was induced by 1 mM isopropyl-1-thio-β-D-galactopyranoside (IPTG) at a culture density OD_{600} of 0.5 to 0.8. The cells were harvested at OD_{600} of 2–3 and were stored as wet pellets at −80 °C.

2.3. Protein purification

The cell pellets (5–10 g) were quick-thawed at 37 °C and were then incubated on ice in 50 mM Tris–HCl, pH 8.2 (5 ml per 1 g of wet pellet) that was supplemented with 1 mM phenylmethylsulphonyl fluoride (PMSF). The cells were broken through repeated passage through an EmulsiFlex-C5 homogenizer (Avestin, Ottawa, Canada). All purification steps thereafter were carried out at 1–4 °C. Cell debris was removed by slow speed centrifugation at 46,000 ×*g* for 30 min and finally bacterial membranes were pelleted by centrifugation at 340,000–360,000 ×*g* for 1 h. The resulting supernatant was decanted and supplemented with 30 mM imidazole, 100 mM NaCl and 1 mM dithiothreitol (DTT). The solution was

applied to a Ni-NTA-agarose (Qiagen) column (2-ml bed volume)) that had been equilibrated with buffer A containing 50 mM Tris–HCl, pH 8.2, 100 mM NaCl and 30 mM imidazole. The column was then washed with 25–30 bed volumes of buffer B (buffer A supplemented with 1 mM DTT) to remove non-specific protein. Subunits *b* or *b′* were eluted with buffer B that had been supplemented with 250 or 300 mM imidazole. The eluant was collected in 1 ml fractions at a flow rate of about 1 ml/min. The protein content was measured according to Bradford [29] using bovine serum albumin as a standard. The fractions with concentrations exceeding 4 mg/ml were combined and stored at −80 °C. Protein purity was verified using 15% polyacrylamide gel electrophoresis [30] in the presence of 0.1% SDS. The protein yield was usually about 20 mg of protein per L bacterial culture.

2.4. Site specific spin labeling

For introduction of the specific spin labels, *b*- and *b′*-subunits were mixed in equimolar ratios at about 0.3 mM each and incubated on ice or at room temperature for 30 min to allow dimerization. To remove DTT that would interfere with the spin-labeling reaction, the protein solution was applied to a 20 ml Sephadex G-25 (Amersham) column (10 mm diameter) that had been equilibrated with a buffer containing 50 mM Tris–HCl, pH 7.5, 10 mM KCl, and 7 mM $MgSO_4$. The sample eluted after about 30 ml of buffer. 0.5-ml fractions were collected at a flow rate of 1.5–2 ml/min. Care was taken that DTT-containing fractions eluted at a later time to avoid contamination of the protein fractions with DTT. A 5–10 fold molar excess (1-oxyl-2,2,5,5-tetramethyl-pyrroline-3-methyl]methanethiosulfonate (MTS) spin label over existing sulfhydryl groups was immediately added to the individual protein fractions and incubated for 1–3 h at 30 °C with. The fractions were then combined and non-reacted spin label was removed by a second passage through a Sephadex G-25 column as described above. Eluted fractions with 0.5–2.5 mg/ml of protein were stored at −80 °C. Denatured protein at any step was removed by centrifugation at 10,000 *g* for 5 min. Alternatively, mutant protein *b* or *b′* was reacted with the spin-label first and then unmodified partner protein was added. Changes in the ESR line-shape of spin-labeled monomeric *b* or *b′* upon addition of un-modified partner protein indicated that dimer formation had taken place (not shown). To assure complete dimer formation, spin labeled *bb′* samples were assayed by SDS electrophoresis [30] for equal contents of *b* and *b′*.

2.5. Electron spin resonance spectroscopy

ESR spectra were acquired using a Bruker EMX 6/1 equipped with a high sensitive cavity ER-4119-HS. All spectra were acquired in the X-band mode with 1 G modulation amplitude at a microwave power of 12.5 mW at room temperature or 4 mW at 223 K. The nitroxide–nitroxide distances were deduced from the acquired low-temperature spectra using a convolution-based method assuming Gaussian distribution of distances as described in detail in Hustedt et al. [31] and according to procedures as described in [32] and [33].

2.6. Molecular modeling of spin-labeled cysteinyl residues

The structures of the MTS spin-labeled cysteine residues were calculated as described in Hornung et al. [25]. Parameters and topology files were created by analogy to the work of Fajer et al. [34]. All hydrogens were included in the simulations and parameterizations.

2.7. Modeling of the bb′-heterodimer coiled coil domain

The *Synechocystis* sp. PCC 6803 *bb′*-heterodimer coiled coil domain was modeled essentially as described in Wise and Vogel [26] with modifications that accommodated the heterodimeric *bb′* interactions. Prediction of heptad repeats in the subunit *b* and *b′* amino acid sequences was performed with the *Paircoil2* program [35] using a sequence window size of 28 residues. Heptad repeats in the cortexillin I coiled coil were predicted using the *Multicoil* program [36]. The VMD program [37] and its the Tcl/Tk [38] and Python [39] interfaces were used for analysis of protein structures. The cortexillin I structure [40] was used as basis for *bb′* modeling. Improved restraint sets were created by measuring distances between heptad *a* and heptad *d* residues in cortexillin I (1D7M, [40]).

The method used inter- and intrachain restraints employed in 2 phases of simulated annealing to generate the structures, followed by refinement and analysis procedures. These restraints were based on interchain Cα to Cα and Cβ to Cβ distances for the interchain atom pairs A*a*1 to B*a*1, Aa1 to Ba2, Ad1 to Bd1, Ad1 to Bd2, Aa1 to Bd1, Aa1 to Bd2 and the intrachain pairs Aa1 to Aa2, Ba1 to Ba2, Ad1–Ad2, Bd1 to Bd2, Aa1 to Ad1, Ba1 to Bd1 (where the first letter denotes the chain, second letter represents the heptad *a* or *d*, and the number indicates the relative position in consecutive heptads with heptad “1” being N-terminal to the heptad labeled “2”) averaged over the 1D7M structure

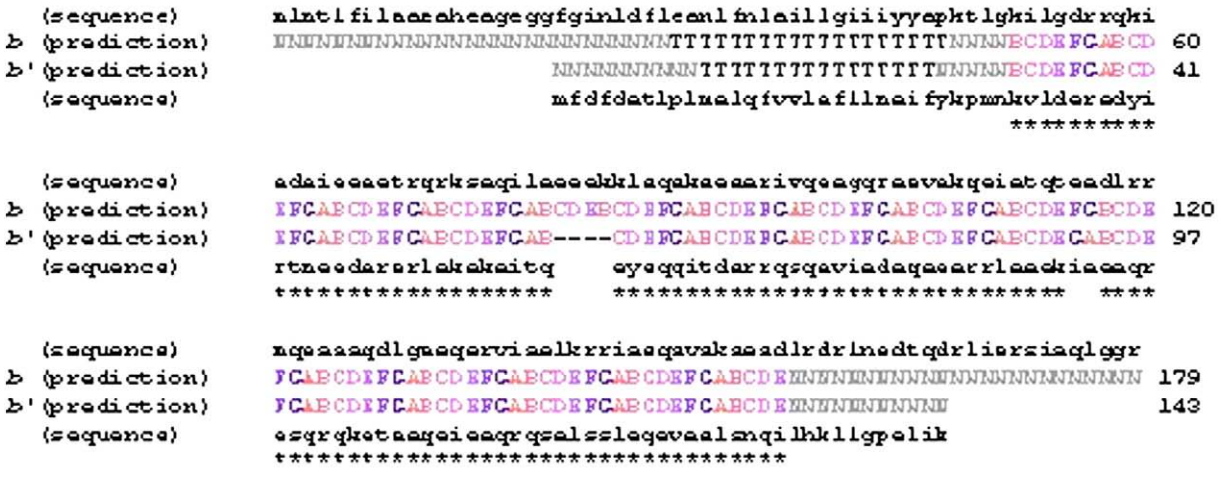

Fig. 1. Proposed alignment of subunits *b* and *b′* in a dimer. The two sequences were aligned using *CLUSTALW* [44] algorithm with an identity matrix according to probable heptad positions (colored upper-case A–G) of amino acid residues (lower-case one-letter code on top of (for subunit *b*) or below (for subunit *b′*) the structure prediction). Hyphen (-) indicates a gap in alignment; star (*) represents a heptad position match; N denotes the residues with lower probability of being in LHCC; T denotes the residues predicted by the program PHDhtm [47,48] to form transmembrane helices.

(Table 2, supporting information). The average distances were then applied to the cortexillin I and subunit *bb′* heptad positions predicted by *Paircoil2* to generate distance restraint tables for the two dimers. The first phase of SA employed only these average Cα to Cα atom distances, as well as φ and ψ dihedrals of 63.7° and 41.7°, respectively and distances between every 10th and 20th Cα atoms to 15 and 30 Å (as in [26]). After refinement, the best model as judged by lowest overall energy calculated by *XPLOR-NIH* was used as a starting template for a second set of simulated annealing calculations that included the Cβ to Cβ distances (Table 2, supporting information) in addition to the first round restraints. Simulated annealing (SA) experiments were performed with *XPLOR-NIH* v. 2.18 [41,42] essentially as described in [26]. Initial models were refined and a subset of acceptable structures was then identified. Acceptable models had no distance restraint or dihedral violations and no angle, dihedral, bond, or improper violation greater than 0.5 Å, 5°, 0.05 Å, or 5°, respectively. *PROCHECK* v. 3.5 [43] was used to assess the quality of some models. A comparison of the model of cortexillin I created by this method and the crystal structure 1D7M [40] can be found in the supplemental information.

When ESR restraints were included, specific residues of the *bb′* dimer were substituted with the spin-labeled cysteine residue and additional SA calculations with the modified residue including restraint data from ESR measurements were performed. Building and minimizing the MTS-labeled cysteine residues for each of the doubly labeled template model proteins was performed for each individual mutation pair in *XPLOR-NIH*. Parameter and topology files for the MTS-labeled cysteine residues were as described [26].

The computers used were Intel Pentium P4 32-bit single CPU units running Scientific Linux 5.0 and a 44-CPU Linux computing cluster with Scientific Linux 5.0 operating systems.

3. Results and discussion

3.1. Prediction of left-handed coiled coil structures from subunit b and b′ sequences

The sequences of 24 subunits *b* and *b′* from different cyanobacterial ATP synthases were analyzed for their propensity to form left-handed coiled coils using the program, *Paircoil2* [35]. The algorithm in *Paircoil2* identifies heptad positions and assigns a probability for participation of any residue in a sequence in a coiled coil heptad. Francis Crick first recognized that left-handed coiled coils would have unique knobs in holes packing interfaces that repeated every 7 residues [27]. Identification of heptad repeats is therefore indicative of the tendency of a protein to form left-handed coiled coil structures. *Paircoil2* assigns each residue a *P*-value that corresponds to the probability of "not" being part of a heptad repeat sequence. Smaller *P*-values therefore give greater confidence that the particular residue under analysis is part of a genuine heptad repeat. The results of *Paircoil2* analyses on the 24 *b* and *b′* sequences showed long extended regions in both *b* and *b′* with *P* values <0.03, indicative of high probabilities that these proteins fold with appropriate partners to form left-handed coiled coil structures (Fig. 4, supporting information).

3.2. Alignment of synechocystis b and b′ heterodimeric heptads

The assigned heptad positions for *Synechocystis* sp. PCC 6803 *b* and *b′* subunits obtained using *Paircoil2* were aligned with *CLUSTALW* [44] to predict complementary heptad pairs (Fig. 1). The observation of extended sequences of heptad complementarity strongly suggested that these proteins form heterodimeric left-handed coiled coil structures. Subunit *b* is longer than subunit *b′* by 36 amino acids. The heptad alignment suggests an N-terminal overhang that is slightly longer than the C-terminal overhand. In Fig. 1 the amino acids are represented with their predicted coiled coil heptad position (A through G). Interestingly, as shown in the figure, there is a gap of four residues in the alignment of subunit *b* and *b′*, with the *b* subunit peptide (*b* residues 80-EEEK-83) having no suitable match in the subunit *b′* sequence (between *b′* residues 60 and 61). The significance of this gap and its effect on the packing interface is discussed below.

3.3. Molecular modeling of left-handed coiled coil structure

The *Synechocystis bb′* structure was modeled using methods originally developed to model the *E. coli* subunit *b* homodimer [26] after including modifications to reflect the heterodimeric nature of *bb′*. In addition to these changes, restraint sets were chosen that tended to

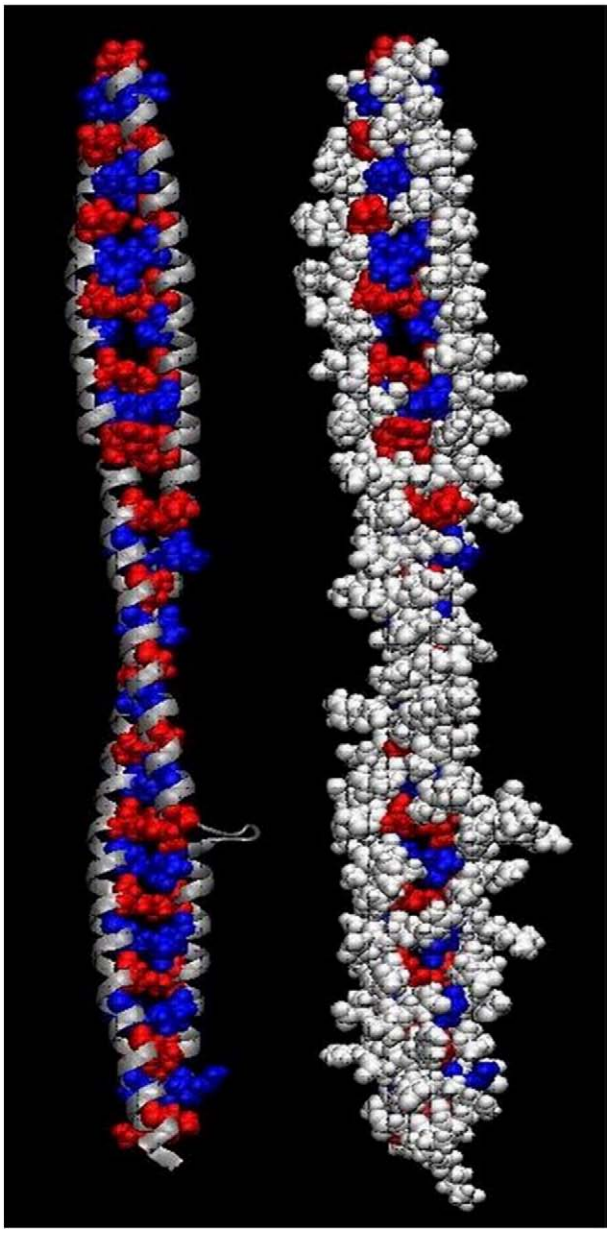

Fig. 2. A left-handed coiled coil dimeric model of the *synechocystis bb′* dimer produced by *ab inition* simulated annealing. Models were created as described in the text. Left. The predominantly helical backbone is shown in silver while heptad *a* residues are shown with blue van der Waal's surfaces and the heptad *d* residues are shown with red surfaces. Right. Residues identified as heptad *b*, *c*, *e*, *f* and *g* were added as white van der Waal's surfaces to the representation.

Table 1A
Intra-*b*′-chain distances at I+8 spacing

Cys-positions	Inter-position spacing	R {ESR} [Å]	R {molecular model} [Å]
b′ 33/41	i,i+8	20.2	20.3
b′ 41/49	i,i+8	>25[a]	26.9
b′ 49/57	i,i+8	>25[a]	24.2
b′ 57/65	i,i+8	14.0/15.9	14
b′ 73/81	i,i+8	21.1	20.3
b′ 81/89	i,i+8	18.1	17.9
b′ 89/97	i,i+8	15.8/18.5	17.9
b′ 97/105	i,i+8	16.6/16.3	16.6
b′ 105/113	i,i+8	16.3	16.3
b′ 113/121	i,i+8	21.5	21.7
b′ 129/137	i,i+8	>25[a]	n.d.

[a] Interspin distances larger than about 25 Å cannot be accurately determined using continuous wave ESR spectroscopy.

Table 1C
Intra-*b*-chain distances at I+4, the mutants in the loop region are highlighted

Cys-positions	Inter-position spacing	R {ESR} [Å]	R {molecular model} [Å]
b 79/83	**i,i+4**	**17.0**	**17.2**
b 83/87	**i,i+4**	**12.0**	**12.0**
b 87/91	**i,i+4**	**16.0**	**15.9**
b 91/95	**i,i+4**	**12.0**	**11.8**
b 114/118	i,i+4	9.3/8.3	8.9
b 118/122	i,i+4	8.1	8.1
b 122/126	i,i+4	12.7/12.9	12.7
b 126/130	i,i+4	11.6/14.1	13.4
b 163/167	i,i+4	20/24	n.d.
b 163/171	i,i+8	13/14	n.d.
b 171/175	i,i+4	21	n.d.
b 171/179	i,i+8	25	n.d.
b 175/179	i,i+4	24	n.d.

better generate complementary heptad knob and hole packing rather than the underwound packing for stuttered coiled coils discussed in [26] and as theoretically described by Brown et al. [45]. Briefly, we chose 6 interchain Cα to Cα and Cβ to Cβ interatomic distances and 6 intrachain Cα to Cα and Cβ to Cβ distances between interface *a* and *d* heptad residues of the left-handed coiled coil dimerization domain of cortexillin I (pdb accession 1D7M [40]) to generate restraint tables for generating the coiled coil models of the cyanobacterial *bb*′ (see Materials and method and the supplemental information for details).

The modeling technique was applied to the *Synechocystis* subunit *b* and subunit *b*′ sequences using the alignment of heptads shown in Fig. 1 to assign heptad *a* and *d* residues that should be packed into "knob and hole" interfaces. Restraint tables for the *b* and *b*′ proteins were built using the distances found in cortexillin I (Materials and methods and supplemental information) in three sections that included subunit *b* residues 53–78 paired with subunit *b*′ residues 34–59, subunit *b* residues 85–113 paired with subunit *b*′ residues 62–90, and subunit *b* residues 119–154 paired with subunit *b*′ residues 96–131. As with the cortexillin I modeling, the dihedral angles in these experiments were restrained to 63.7° and 41.7° for φ and ψ angles, respectively, and every 10th and 20th Cα atoms were restrained to 15 and 30 Å [26]. Initially, 46 structures were built using these restraints and the cortexillin I Cα atom pair distances (Table 2A, supplemental information). After refinement, eleven acceptable models were found. These 11 models were then used as templates to build models using both Cα atom to Cα atom restraints and the Cβ atom to Cβ atom restraints (Table 2B, supplemental information). Forty-six structures for each of the eleven models were built and refined in these runs. After analysis for stereochemical quality, 351 of the resultant models were found to be acceptable. The summary data on these structures is shown in Table 5, supporting information. The model with the lowest energy as measured by *XPLOR-NIH* (Materials and methods) was chosen for use in the remainder of this study.

Fig. 2 presents two graphical representations of the lowest energy left-handed, dimeric coiled coil model for *bb*′ produced in these experiments. This model when checked with the *PROCHECK* v3.5 program suite showed 95.4% of the residues with core and 3.6% with allowed Ramachandran values and an overall G-factor value of 0.38. In the left panel, the backbone helices are shown in cartoon form with the packing interface heptad *a* residues shown in blue surface representations and the interface heptad *d* residues shown with red surfaces. The right panel shows the heptad *b*, *c*, *e*, *f* and *g* residues in white surface representations in addition to the packing interfaces.

The loop of residues 80 through 83 in subunit *b* caused by the gap in the heptad alignment (Fig. 1) is evident in the lower right-hand side of both panels of Fig. 2 (a close up is shown in the left-hand panel of Fig. 6, supporting information). This non-helical 4 residue section of subunit *b* may give the *b* protein sufficient flexibility that the knobs and holes packing can continue through this section of the model without causing any major discontinuity in the packing interface. The two residues out of 204 total with Ramachandran values outside of the *PROCHECK* 3.5 allowed averages were from subunit *b* residues 82 and 83 and may reflect the tightness of the heptad *a* and *d* restraints on either side of the loop. Cain et al. have created a number of variants of the *E. coli* subunit *b* dimer with peptide substitutions, deletions and insertions in coiled coil regions that assemble active, functional ATP synthases. The *Synechocystis* subunit *bb*′ model presented here might explain how the mutant subunit *b* dimers of Cain et al. [16,17,19] and more recently from Dunn et al. [46] can be compensated without causing a complete breakdown in packing of the dimer.

Table 1B
Intra-*b*′-chain distances at I+4, I+6 and I+7 spacing

Cys-positions	Inter-position spacing	R {ESR} [Å]	R {molecular model} [Å]
b′ 49/53	i,i+4	14.9/13.8	14.3
b′ 73/77	i,i+4	10.1	10.0
b′ 82/89	i,i+7	14.1	13.8
b′ 89/93	i,i+4	11.5	11.7
b′ 89/95	i,i+6	18.2	18.0
b′ 89/96	i,i+7	11.0/13.2	11.0
b′ 105/112	i,i+7	18.0	17.6
b′ 129/133	i,i+4	22.4/>25[a]/14.7	n.d
b′ 137/141	i,i+4	18.0	n.d.

[a] Interspin distances larger than about 25 Å cannot be accurately determined using continuous wave ESR spectroscopy.

Table 1D
Inter-b-b′ distances

Cys-positions	Predicted heptad position	R {ESR} [Å]	R {molecular model} [Å]
b 67-*b*′ 49	*d-e*′	16.7/22.0	18.8
b 70-*b*′ 49	*g-e*′	>25[a]	24.7
b 99-*b*′ 77	*d-e*′	18.0	17.7
b 102-*b*′ 77	*g-e*′	20.1	19.7
b 128-*b*′ 105	*f-f*′	24.1	27.1
b 133-*b*′ 111	*d-e*′	>25[a]	24.6
b 136-*b*′ 111	*g-e*′	>25[a]	25.0
b 163-*b*′ 137	N/A	>25[a]	n.d.
b 171-*b*′ 137	N/A	>25[a]	n.d.
b 179-*b*′ 137	N/A	23.5	n.d.

[a] Interspin distances larger than about 25 Å cannot be accurately determined using continuous wave ESR spectroscopy.

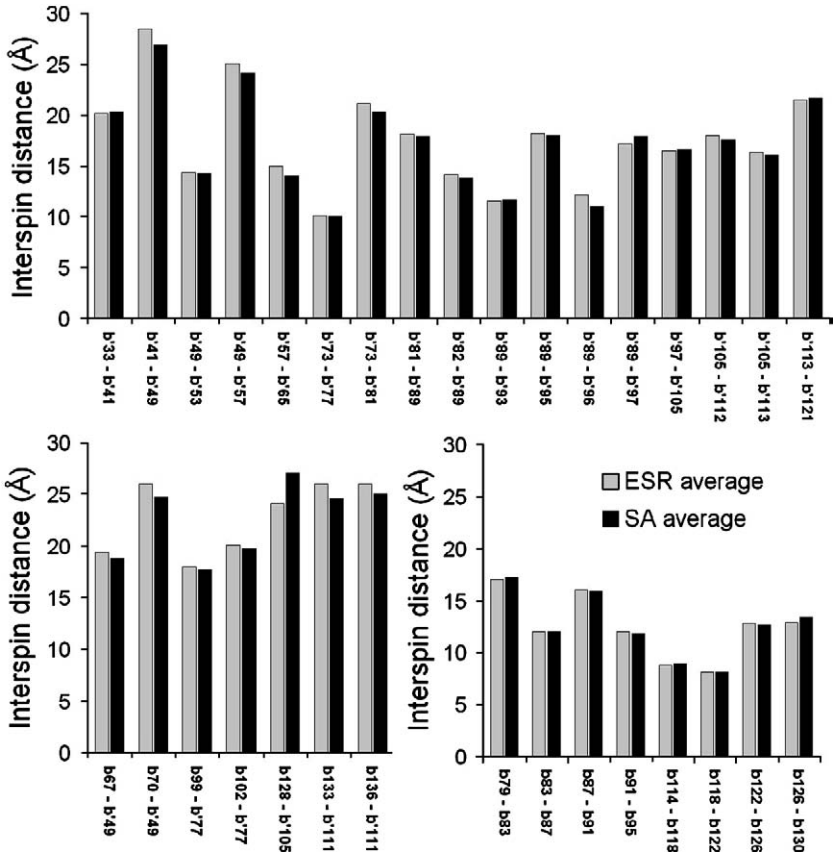

Fig. 3. Comparisons of the MTS inter-radical distances calculated from ESR measurements or determined in simulated annealing models of site-specifically spin-labeled proteins. Inter-radical distances are presented on the *Y*-axis and the mutation identifiers are presented on the *X*-axis. In no case was the difference between ESR determined and simulated annealing modeled inter-radical distances greater than 10% of the ESR-determined value.

Also of interest in the *Synechocystis bb′* model, Fig. 2, are the adjacent heptad *d* pairs at *b113-b′90* and *b119-b′96* that have no intervening heptad *a* pair between them. A close-up of this section of the model is given in Fig. 6, right panel (supporting information). While the *Paircoil2* program did identify subunit *b′* Ala-93 as an "*a*" heptad (Fig. 1 and Fig. 6 right, supporting information), subunit *b* Ala-116 (across from *b′*-93, white, same figure) was predicted to be a "*g*" heptad. This was apparently caused by the single residue discontinuity at *b116-117* and *b′92-93* in the identified heptad positions that results in a 6-residue spacing between the adjacent *d* residues instead of the normal 7-residue heptad spacing. Neither *XPLOR-NIH* nor *PROCHECK* found any incongruous or disallowed structural geometries in this region. While the heptad *d* pair that directly precedes the anomaly does interact as expected for a coiled coil (Fig. 6 right, supplemental information), the heptad *d* pair that directly follows the anomaly (*b119* and *b′96*) does not pack into a classic knob and hole interface, likely the consequence of the 6-residue spacing between these *d* heptad pairs. Normal coiled coil packing resumes with the heptad *a* pair that follows (residue *b123-b′100*).

3.4. Determination of intra and inter-chain distances between site-specifically introduced spin labels by ESR spectroscopy

We generated a total of 43 individual double cysteine mutations by conventional site directed mutagenesis techniques in either subunit *b*, subunit *b′* or in *b* and *b′* in combination. The mutants were spaced at intervals of either 4, 6, 7 or 8 amino acids along either one of the peptide chains or at positions where we either assumed peptide packing would occur or, as negative controls, those where we did not predict packing interactions would occur. The cysteine mutants were reacted with MTS-spin-label as described in Hornung et al. [25] and Materials and methods. ESR spectra were acquired at 223 K in frozen solutions. A set of typical ESR spectra of double labeled *bb′*, with either intra- or intermolecular attachment of spin-labels is given in Fig. 7 of the supplemental information. A series of mutants was generated in the *b′* subunit with an inter-mutation spacing of 8 amino acids (I+8) and the corresponding spectra were acquired as described in Materials and methods. The I+8 spacing was chosen to reflect a little more than two helical turns. This I+8 spacing allowed us to still detect dipolar interactions between the spins using continuous wave ESR spectroscopy while slowly turning the spin labels out of a potential helical interface when moving up the helix.

Table 1A lists I+8 interspin distances that were obtained after simulating the acquired ESR spectra and extracting the dipolar line broadening as described in Materials and methods. Most of the I+8 distances were between 16 and 22 Å, suggesting a somewhat deformed helical structure of *b′* as would be expected for a helix participating in a coiled coil packing. Tables 1B and C list interspin distances at the shorter I+4 (about one helical turn), I+6 (about one and a half helical turns) and I+7 (about two helical turns) intervals. Double mutants in both *b* and *b′* showed I+4 distances of between 8 and 12 Å, I+7 distances were an average of 14 Å and I+6 was slightly larger at 18 Å. In all cases, the interspin distances obtained by ESR spectroscopy measurements correlated very well, usually with less than 0.5 Å deviations, with interspin distances obtained through molecular modeling as is described below. It should be pointed out that also in the loop region predicted for subunit *b*, see Fig. 2 or Fig. 6 (supporting information, left panel), and as highlighted in Table 1C the acquired and modeled inter-spin distances correlated extremely well, with deviations less than 0.2 Å.

In the C-terminal region of both *b* and *b′* the distances obtained by ESR were very irregular (some very long distances for I+4 and some very short for I+8) suggesting that the C-terminal regions of both proteins are not strictly folded as extended α-helices (Table 1A, B and C). These parts of the proteins were not included in the molecular modeling since coiled coil formation was not predicted (Fig. 1 and Fig. 4, supplemental information). Again and as seen in more detail below, ESR-determined structural data correlated well with the predictions obtained by the programs applied and models created in this study.

3.5. Distances determined by spin labeling correspond well and support the left-handed coiled coil model

Modeling of the spin labeled subunit *bb′* dimers that were experimentally obtained as described above was achieved by simulated annealing experiments using MTS-derivatized cysteine residues at the desired mutation sites, see Materials and methods. The best subunit *bb′* model described above (Fig. 2) was used as a starting template for the simulated annealing experiments after substitution of the side chains at the desired spin-labeling sites in the template with the MTS-derivatized cysteine residue. This was accomplished by first building the residues and then minimizing the mutated side chains with scripts run in *XPLOR-NIH*. Individually doubly-spin labeled template structures were then used in simulated annealing experiments that included all the restraints employed in generating the models shown in Fig. 2 (and Table 5, supplemental information) as well as distance restraints derived from the inter-spin distances measured from the ESR experiments described above. The spin–spin restraints were given an upper and lower range limit of 10% of the measured distance, above which restraint violations would be tabulated. In this way, we were able to test whether the ESR measured MTS to MTS distances for the two mutations could be accommodated in left-handed coiled coil structures related to that shown in Fig. 2.

Results of these experiments are shown in Fig. 3 where they are compared to interspin distances directly measured by ESR spectroscopy. In all, 32 different combinations of two MTS labeled residues in either intra-chain combinations, *i.e.* in subunit *b′* alone (Fig. 3, top panel) or in subunit *b* alone (Fig. 3, bottom right) or in inter-chain combinations in both subunit *b* and subunit *b′* (Fig. 3, bottom left) were modeled and refined using the methods described above. Out of 1472 resultant independently produced models (46 structures generated per experiment with 32 different combinations of two MTS-labeled cysteine substituted residues), none of the modeled structures had any violations of the ESR-determined radical distances nor did any of the 1472 models display any other distance or dihedral restraint violations. All of the 1472 structures were judged by *XPLOR-NIH* acceptance analyses to be geometrically normal in that none of the structures showed any angle, dihedral, bond, or improper violation greater than 0.5 Å, 5°, 0.05 Å, or 5°, respectively.

4. Conclusion

The ability of the modeled subunit *bb′* structures to accommodate the independently measured ESR distance data between 32 different pairs of MTS spin-label derivatized cysteine mutations presented here very strongly supports the hypothesis that the *Synechocystis* subunit *bb′* dimer can fold into a stable, classically described, left-handed coiled coil protein.

Acknowledgments

The authors would like to acknowledge the support of Joseph Gargiula, Abby Kinney, Allen Hughes, Randall Powell, JoAnn Lan, Justin Ross and James Jaeger of Information Technology Services at Southern Methodist University for the computers used in this work and to Justin Ross for his invaluable expertise in setting up and maintaining the computing cluster.

Appendix A. Supplementary data

Supplementary data associated with this article can be found, in the online version, at doi:10.1016/j.bbabio.2008.12.007.

References

[1] P.D. Boyer, The ATP synthase — a splendid molecular machine, Annu. Rev. Biochem. 66 (1997) 717–749.
[2] P.D. Boyer, ATP synthase — past and future, Biochim. Biophys. Acta 1365 (1998) 3–9.
[3] ATP Synthesis by Oxidative Phosphorylation.
[4] J.E. Walker, V.K. Dickson, The peripheral stalk of the mitochondrial ATP synthase, Biochim. Biophys. Acta 1757 (2006) 286–296.
[5] J. Weber, ATP synthase: subunit–subunit interactions in the stator stalk, Biochim. Biophys. Acta 1757 (2006) 1162–1170.
[6] J. Weber, ATP synthase — the structure of the stator stalk, Trends Biochem. Sci. 32 (2007) 53–56.
[7] J. Weber, S. Wilke-Mounts, S. Nadanaciva, A.E. Senior, Quantitative determination of direct binding of b subunit to F1 in *Escherichia coli* F_1F_0–ATP synthase, J. Biol. Chem. 279 (2004) 11253–11258.
[8] K. Shimabukuro, R. Yasuda, E. Muneyuki, K.Y. Hara, K.J. Kinosita, M. Yoshida, Catalysis and rotation of F1 motor: cleavage of ATP at the catalytic site occurs in 1 ms before 40 degree substep rotation, Proc. Natl. Acad. Sci. U. S. A. 100 (2003) 14731–14736.
[9] H. Ueno, T. Suzuki, K.J. Kinosita, M. Yoshida, ATP-driven stepwise rotation of F_0F_1–ATP synthase, Proc. Natl. Acad. Sci. U. S. A. 102 (2005) 1333–1338.
[10] R. Yasuda, H. Noji, M. Yoshida, K.J. Kinosita, H. Itoh, Resolution of distinct rotational substeps by submillisecond kinetic analysis of F1-ATPase, Nature 410 (2001) 898–904.
[11] D.A. Cherepanov, W. Junge, Viscoelastic dynamics of actin filaments coupled to rotary F-ATPase: curvature as an indicator of the torque, Biophys. J. 81 (2001) 1234–1244.
[12] W. Junge, O. Pänke, D.A. Cherepanov, K. Gumbiowski, M. Müller, S. Engelbrecht, Inter-subunit rotation and elastic power transmission in F0F1-ATPase, FEBS Lett. 504 (2001) 152–160.
[13] R.J. Carbajo, J.A. Silvester, M.J. Runswick, J.E. Walker, D. Neuhaus, Solution structure of subunit F(6) from the peripheral stalk region of ATP synthase from bovine heart mitochondria, J. Mol. Biol. 342 (2004) 593–603.
[14] R.J. Carbajo, F.A. Kellas, M.J. Runswick, M.G. Montgomery, J.E. Walker, D. Neuhaus, Structure of the F1-binding domain of the stator of bovine F1Fo-ATPase and how it binds an alpha-subunit, J. Mol. Biol. 351 (2005) 824–838.
[15] R.J. Carbajo, F.A. Kellas, J. Yang, M.J. Runswick, M.G. Montgomery, J.E. Walker, D. Neuhaus, How the N-terminal domain of the OSCP subunit of bovine F_1F_0–ATP synthase interacts with the N-terminal region of an alpha subunit, J. Mol. Biol. 368 (2007) 310–318.
[16] P.L. Sorgen, T.L. Caviston, R.C. Perry, B.D. Cain, Deletions in the second stalk of F_1F_0–ATP synthase in *Escherichia coli*, J. Biol. Chem. 273 (1998) 27873–27878.
[17] P.L. Sorgen, M.R. Bubb, B.D. Cain, Lengthening the second stalk of F(1)F(0) ATP synthase in *Escherichia coli*, J. Biol. Chem. 274 (1999) 36261–36266.
[18] T.B. Grabar, B.D. Cain, Integration of b subunits of unequal lengths into F_1F_0–ATP synthase, J. Biol. Chem. 278 (2003) 34751–34756.
[19] S.B. Claggett, T.B. Grabar, S.D. Dunn, B.D. Cain, Functional incorporation of chimeric b subunits into F_1F_0 ATP synthase, J. Bacteriol. 189 (2007) 5463–5471.
[20] C. Motz, T. Hornung, M. Kersten, D.T. McLachlin, S.D. Dunn, J.G. Wise, P.D. Vogel, The subunit b dimer of the F_0F_1–ATP synthase: interaction with F1-ATPase as deduced by site-specific spin-labeling, J. Biol. Chem. 279 (2004) 49074–49081.
[21] P.A. Del Rizzo, Y. Bi, S.D. Dunn, B.H. Shilton, The "second stalk" of *Escherichia coli* ATP synthase: structure of the isolated dimerization domain, Biochemistry 41 (2002) 6875–6884.
[22] A. Lupas, Predicting coiled-coil regions in proteins, Curr. Opin. Struct. Biol. 7 (1997) 388–393.
[23] P.A. Del Rizzo, Y. Bi, S.D. Dunn, ATP synthase b subunit dimerization domain: a right-handed coiled coil with offset helices, J. Mol. Biol. 364 (2006) 735–746.
[24] K.S. Wood, S.D. Dunn, Role of the asymmetry of the homodimeric b2 stator stalk in the interaction with the F1 sector of *Escherichia coli* ATP synthase, J. Biol. Chem. 282 (2007) 31920–31927.
[25] T. Hornung, O.A. Volkov, T.M.A. Zaida, S. Delannoy, J.G. Wise, P.D. Vogel, Structure of the Cytosolic Part of the Subunit b-Dimer of *Escherichia coli* F_0F_1–ATP Synthase, Biophys. J. 94 (2008) 5053–5064.
[26] J.G. Wise, P.D. Vogel, Subunit b-dimer of the *Escherichia coli* ATP synthase can form left-handed coiled-coils, Biophys. J. 94 (2008) 5040–5052.
[27] F.H.C. Crick, The packing of alpha-helices: simple coiled-coils, Acta Cryst. 6 (1953) 689–697.
[28] S.D. Dunn, E. Kellner, H. Lill, Specific heterodimer formation by the cytoplasmic domains of the b and b′ subunits of cyanobacterial ATP synthase, Biochemistry 40 (2001) 187–192.
[29] M.M. Bradford, A rapid and sensitive method for the quantitation of microgram quantities of protein utilizing the principle of protein–dye binding, Anal. Biochem. 72 (1976) 248–254.

[30] U.K. Laemmli, Cleavage of structural proteins during the assembly of the head of bacteriophage T4, Nature 227 (1970) 680–685.
[31] E.J. Hustedt, R.A. Stein, L. Sethaphong, S. Brandon, Z. Zhou, S.C. Desensi, Dipolar coupling between nitroxide spin labels: the development and application of a tether-in-a-cone model, Biophys. J. 90 (2006) 340–356.
[32] H.J. Steinhoff, N. Radzwill, W. Thevis, V. Lenz, D. Brandenburg, A. Antson, G. Dodson, A. Wollmer, Determination of interspin distances between spin labels attached to insulin: comparison of electron paramagnetic resonance data with the X-ray structure, Biophys. J. 73 (1997) 3287–3298.
[33] M.D. Rabenstein, Y.K. Shin, Determination of the distance between two spin labels attached to a macromolecule, Proc. Natl. Acad. Sci. U. S. A. 92 (1995) 8239–8243.
[34] K. Sale, C. Sár, K.A. Sharp, K. Hideg, P.G. Fajer, Structural determination of spin label immobilization and orientation: a Monte Carlo minimization approach, J. Magn. Reson. 156 (2002) 104–112.
[35] A.V. McDonnell, T. Jiang, A.E. Keating, B. Berger, Paircoil2: improved prediction of coiled coils from sequence, Bioinformatics 22 (2006) 356–358.
[36] E. Wolf, P.S. Kim, B. Berger, MultiCoil: a program for predicting two- and three-stranded coiled coils, Protein Sci. 6 (1997) 1179–1189.
[37] Humphrey W, Dalke A & Schulten K. VMD: visual molecular dynamics. J. Mol. Graph. (1996) 14: p. 33–8, 27–8.
[38] Ousterhout J. Tcl and t he Tk Toolkit. Addison-Wesley Professional, Upper Saddle River, NJ, 1994.
[39] M.F. Sanner, Python: a programming language for software integration and development, J. Mol. Graph. Model. 17 (1999) 57–61.
[40] P. Burkhard, R.A. Kammerer, M.O. Steinmetz, G.P. Bourenkov, U. Aebi, The coiled-coil trigger site of the rod domain of cortexillin I unveils a distinct network of interhelical and intrahelical salt bridges, Structure 8 (2000) 223–230.
[41] M. Nilges, J. Kuszewski, A.T. Brünger, Sampling properties of simulated annealing and distance geometry, in: J.C. Hoch, F.M. Poulsen, C. Redfield (Eds.), Computational Aspects of the Study of Biological Macromolecules by NMR, 1991, pp. 451–455.
[42] C.D. Schwieters, J.J. Kuszewski, N. Tjandra, G.M. Clore, The Xplor-NIH NMR molecular structure determination package, J. Magn. Reson. 160 (2003) 65–73.
[43] R.A. Laskowski, J.A. Rullmannn, M.W. MacArthur, R. Kaptein, J.M. Thornton, AQUA and PROCHECK-NMR: programs for checking the quality of protein structures solved by NMR, J. Biomol. NMR 8 (1996) 477–486.
[44] J.D. Thompson, D.G. Higgins, T.J. Gibson, CLUSTAL W: improving the sensitivity of progressive multiple sequence alignment through sequence weighting, position-specific gap penalties and weight matrix choice, Nucleic Acids Res. 22 (1994) 4673–4680.
[45] J.H. Brown, C. Cohen, D.A. Parry, Heptad breaks in alpha-helical coiled coils: stutters and stammers, Proteins 26 (1996) 134–145.
[46] Y. Bi, J.C. Watts, P.K. Bamford, L.K. Briere, S.D. Dunn, Probing the functional tolerance of the b subunit of *Escherichia coli* ATP synthase for sequence manipulation through a chimera approach, Biochim. Biophys. Acta (in press).
[47] B. Rost, R. Casadio, P. Fariselli, C. Sander, Transmembrane helices predicted at 95% accuracy, Protein Sci. 4 (1995) 521–533.
[48] B. Rost, PHD: predicting one-dimensional protein structure by profile-based neural networks, Methods Enzymol. 266 (1996) 525–539.